



The mobilization of debris flows from shallow landslides

Emmanuel J. Gabet ^{a,*}, Simon M. Mudd ^b

^a *Department of Geology, University of Montana, Missoula, MT 59812, USA*

^b *Department of Civil and Environmental Engineering, Vanderbilt University, Nashville, TN 37235, USA*

Received 16 February 2005; received in revised form 1 August 2005; accepted 2 August 2005

Abstract

According to critical state theory, a soil will approach a critical void ratio during shear such that loose soils contract and dense soils dilate. Theory indicates that failing soils must be loose to generate the pore pressures needed for the mobilization of debris flows. Previously published results from large-scale experiments have also suggested that soils must be initially loose to fail as debris flows. In this contribution, this mechanism for soil liquefaction is tested in the field through observations and geotechnical analysis of soils that failed during a large storm in central California. Surprisingly, we find that the debris flows mobilized from soils that were initially dense. In addition, we find that the potential for debris flow mobilization was strongly linked to the fines/sand ratio. We present results from a numerical model that indicate that, as dilational soils approach the critical void ratio, the arresting effect of negative pore pressures generated by dilation is greatly reduced, leading to a rapid increase in basal pore pressure and rapid downslope acceleration. In addition, the model results suggest that the downslope displacement required to reach the critical state porosity in a dilative soil will be on the order of 0.1 to 1 m. Because the rate of the approach to critical state is fundamentally a function of the hydraulic conductivity of the soil, sandy soils will approach critical state much more rapidly than clay-rich soils.

© 2005 Elsevier B.V. All rights reserved.

Keywords: Debris flow; Landslide; Liquefaction; Critical-state porosity; Natural hazard

1. Introduction

By virtue of their velocities and their sizes, debris flows are important geomorphological agents. Debris flows are the most destructive type of landslide and have caused the most deaths (Alexander, 1989) and as the urban fringe around the world continues to encroach into the surrounding foothills and mountains, the potential loss of life and property from debris flows will escalate (Gares et al., 1994). In steep

terrain, debris flows are also important sources of sediment to channel networks (Benda and Dunne, 1997; Gabet and Dunne, 2003), altering stream morphology and affecting aquatic habitats (Benda et al., 2003). Over longer time scales, debris flows may control the morphological evolution of steep catchments (Stock and Dietrich, 2003).

Most debris flows begin as rigid translational slides that liquefy (Iverson et al., 1997), but this process is poorly understood. Early attempts to explain this transformation proposed that a failing soil behaves like a Bingham viscoplastic (Johnson, 1996). The Bingham model is attractive because it is characterized by a yield strength, which has been interpreted as “a material property denoting the transition between ‘solid-like’

* Corresponding author. Tel.: +1 406 543 0309; fax: +1 406 543 4028.

E-mail address: manny.gabet@mso.umt.edu (E.J. Gabet).

48 and ‘liquid-like’ behavior” (Doraiswamy et al., 1991, p.
49 648). The Bingham model, however, has been criticized
50 as an inappropriate and oversimplified analog for soil
51 behavior (see Iverson et al., 1997 for a thorough re-
52 view). Presently, the prevailing theory proposed to
53 explain debris flow mobilization traces its roots to
54 work done by Casagrande (1936) who found that, if a
55 drained soil is continually sheared, it will eventually
56 attain a critical-state (i.e., steady-state) porosity. Loose
57 soils will contract to reach the critical-state porosity and
58 dense soils will dilate (Fig. 1).

59 Several studies have invoked critical-state theory to
60 explain the mobilization of debris flows. Sassa (1984)
61 concluded that this mechanism was responsible for the
62 liquefaction of loose sand in laboratory experiments. In
63 relatively undrained conditions (i.e., when pore water is
64 unable to enter or leave the soil mass rapidly enough),
65 dilative and contractive tendencies of the soil result in
66 changes in pore pressure during shear because water is
67 incompressible. Iverson et al. (2000) demonstrated,
68 through large-scale flume experiments, that the shear-
69 ing of a loose loamy sand triggered rapid pore pressure
70 increases because, as the soil began to collapse, the
71 weight of the soil was shifted onto the pore fluid. This
72 abrupt increase in pore pressure resulted in immediate
73 liquefaction of the experimental soil. In addition, Iver-
74 son et al. (2000) found that the same loamy sand, but

75 densely packed, exhibited dilative tendencies during
76 failure, thus reducing pore pressures and inhibiting
77 mobilization.

78 During the winter of 1997–1998, Sedgwick Re-
79 serve, in the central coast region of California (Fig.
80 2), lay in the path of a series of El Niño-generated
81 rainstorms. In February, 21 cm of rain fell in a 48-
82 h period (Fig. 3), triggering over 150 shallow soil
83 failures in a 10 km² area vegetated by both coastal
84 sage scrub and grasslands (Gabet and Dunne, 2002).
85 On the grass-covered slopes, about half (56%) of the
86 failures mobilized as debris flows, whereas many of
87 the other failures moved only a few meters before
88 stopping as slumps, sensu Kesseli (1943) (Fig. 4).
89 This presented an ideal opportunity to test the criti-
90 cal-state porosity theory for debris flow mobilization.
91 We hypothesized that the soils that produced debris
92 flows were contractive and those that produced the
93 slumps were dilative. To test this hypothesis, we
94 analyzed soil samples taken from the sites of a subset
95 of these shallow failures.

96 2. Methods

97 2.1. Field site and surveys

98 The field site, Sedgwick Reserve, is located on the
99 margin of the Santa Ynez valley, ~60 km north of Santa
100 Barbara, CA. The climate is subhumid, Mediterranean.
101 The bedrock is a Pliocene fanglomerate (Dibblee,
102 1993).

103 The failures were inspected several weeks after
104 they occurred. In both the slumps and the debris
105 flows, the soil–bedrock boundary defined the failure
106 plane. The failures that mobilized as debris flows
107 completely evacuated the scars (Figs. 4 and 5). In
108 the slumps, the displacement of the center of mass
109 ranged from 1 to 2 m, and the failing mass never
110 overrode the soil surface downslope of the failure
111 (Figs. 4 and 5).

112 During the spring of 1998, the recent landslides
113 were mapped from aerial photos. Thirty-two of these
114 landslides were surveyed to measure hillslope angle
115 and to estimate volumes of sediment evacuated (Gabet
116 and Dunne, 2002). From this initial set, we selected
117 failures in the grassland that met two criteria. First, to
118 control for the effect of hillslope angle on debris flow
119 mobilization, only failures that occurred on slopes
120 within a narrow range of angles were chosen and the
121 range of slope angles with the highest density of fail-
122 ures was 28° to 32°. Second, to ensure a relatively
123 uniform spatial rainfall distribution, only failures in

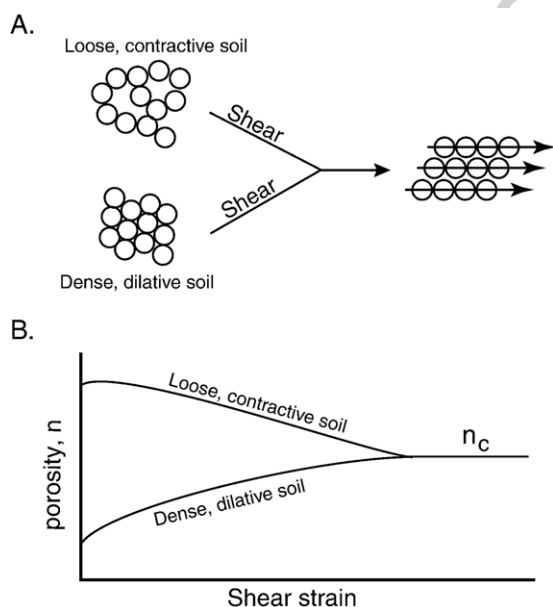


Fig. 1. (A) Under drained conditions, loose soils collapse during shear, whereas dense soils must dilate to overcome the resistance from the interlocking of grains. (B) During shear, both contractive and dilative soils eventually reach a constant critical porosity, n_c (modified from Iverson, 1997).

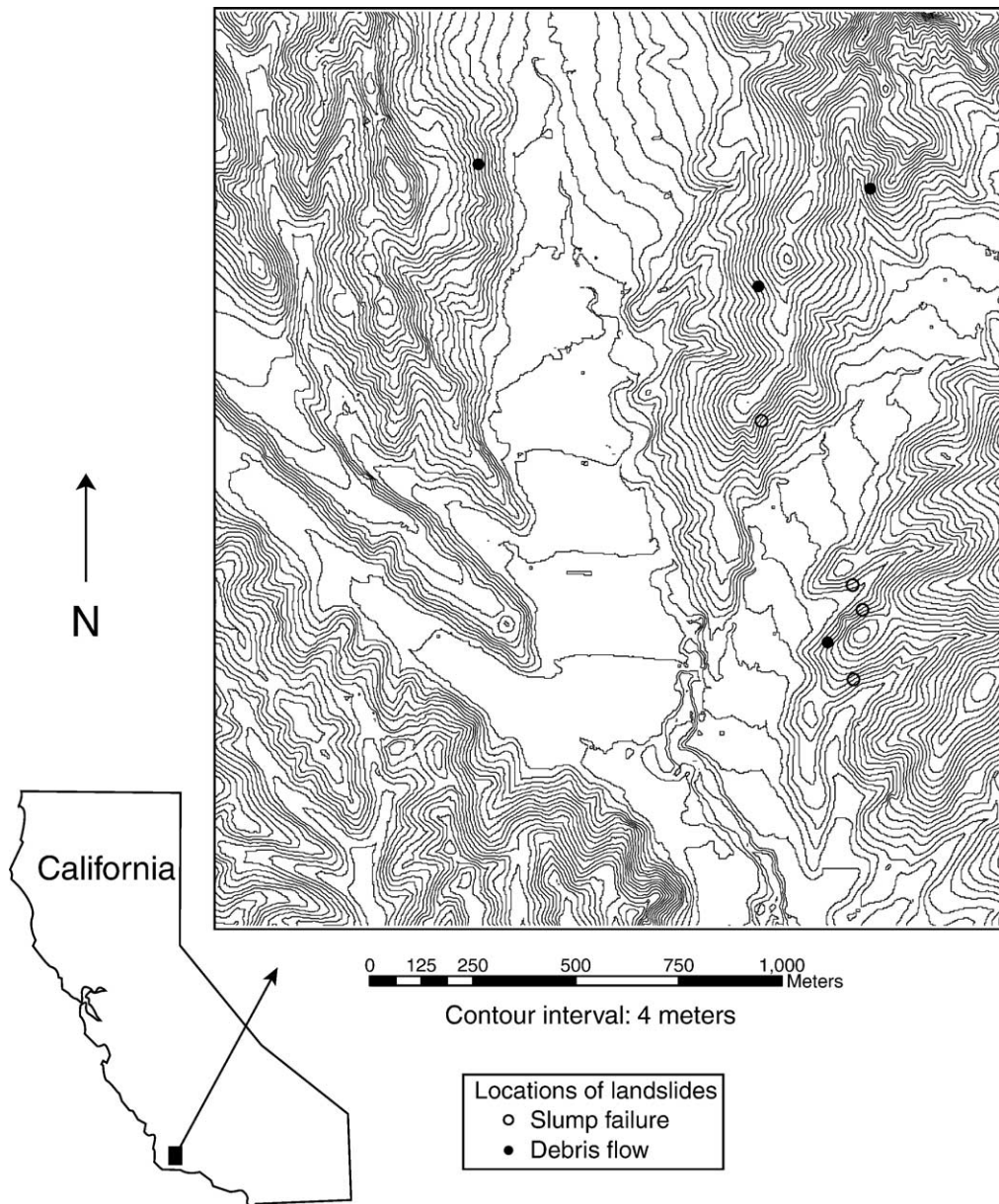


Fig. 2. Location of the field site in central California. Locations of slope failures indicated on topographic map. Contour labels omitted for clarity: minimum elevation=320 m, maximum elevation=669 m. Flat, broad features are valley bottoms.

124 close proximity to each other were chosen. Four debris
 125 flows and four slumps within a 1.2-km² area met these
 126 conditions.

127 Because the degree of saturation of the soils at
 128 failure could have had an important effect on liquefac-
 129 tion potential, the topographic index (Beven and
 130 Kirkby, 1979), a measure of potential saturation, was
 131 calculated for each failure according to

$$\text{Top. index} = \ln\left(\frac{a/w}{\tan\theta}\right) \quad (1)$$

where w is the failure width, a is the contributing area
 upslope of the failure (measured from the margins of
 the failure), and θ is the hillslope angle.

2.2. Texture and porosity

A total of two soil samples, taken on either lateral
 margin of the failure scar (Fig. 4), were collected from
 each site. For consistency, the sampling depth was ap-
 proximately halfway between the soil surface and the
 slip plane (~0.25 m). The sand fraction was measured by

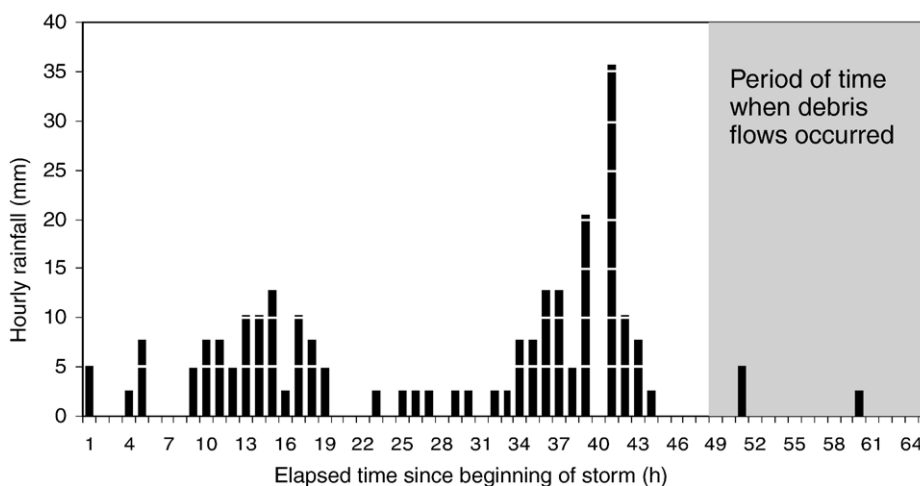


Fig. 3. Hourly rainfall from the storm that triggered the landslides. Before this storm, 140 mm of rain had fallen in the previous 30 days. Because the debris flows occurred at night, we are only unable to bracket a time interval during which they must have occurred (shaded area). Note that the debris flows did not occur during the period of highest rainfall intensity. Rainfall data from Figueroa Mountain Ranger Station (elevation 976 m), 3 km NE of Sedgwick Ranch; the difference in elevation suggests that the rainfall intensities might have been less at Sedgwick Ranch.

142 sieving, drying, and weighing. The silt and clay fractions
 143 were determined with a Mastersizer™ automatic particle
 144 size analyzer. Particle size data from the two samples
 145 taken at each landslide scar were averaged.

146 Dry bulk densities (ρ_b) of the soil samples were
 147 measured using the resin-coated clod technique (Brasher

et al., 1966). Soil sample volumes were measured with
 saturated samples to account for volume expansion from
 the presence of shrink–swell clays. The porosity (n) of
 each sample was calculated with:

$$n = 1 - \frac{\rho_b}{\rho_m} \quad (2)$$

where ρ_m , the density of the mineral grains, was assumed to be 2.65 g/cm³.

2.3. Constant-shear-drained tests

Soil samples were collected within 1 m of the failure
 scars of two debris flow failures and two slumps.
 Samples were obtained by carefully pushing 71-mm
 diameter, 200-mm-long tubes into the soil at approxi-
 mately 50 cm depth; soil was then carved away from
 the outside and bottom of each tube. The samples were
 collected shortly after a rainstorm to minimize the
 disruption that might have occurred by pushing the
 core-tubes into a dry, brittle soil. Although the soil
 immediately adjacent to the core-tubes may have been
 compressed while retrieving the sample, the bulk of the
 sample did not appear to be disturbed by the procedure.
 Care was taken to ensure that the samples were from
 areas that had not undergone any strain. The samples
 were extruded vertically at the UC Berkeley Geotechni-
 cal Laboratory and tested using the constant-shear-
 drained (CSD) method described in Reimer (1992).

The testing of soils to understand their behavior
 during shallow failures requires a method that mimics
 the stress field under natural conditions. Shallow land-
 slides are triggered by elevated pore pressures that

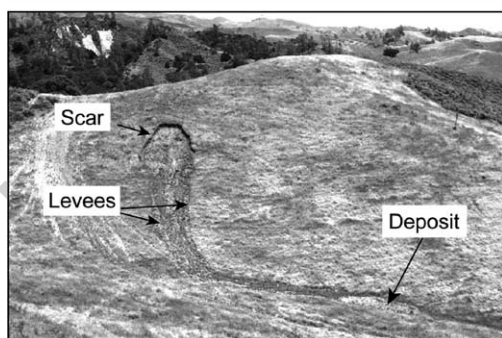
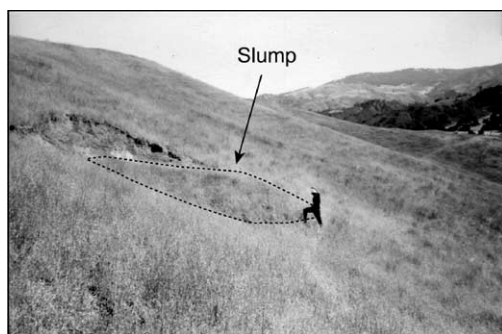


Fig. 4. Top: Slump where the failing mass only moved several meters. Dotted line outlines the slide mass. Bottom: Failing mass liquified as a debris flow, completely evacuated the scar, and flowed down to the valley bottom.

177 decrease the effective normal stress (i.e., the normal
 178 load minus the pore pressure) rather than by an increase
 179 in the shear stress (Anderson and Reimer, 1995).
 180 Whereas typical triaxial shear testing is done by in-
 181 creasing the shear stress, the CSD test approximates the
 182 conditions during rainfall-induced failure by holding
 183 the shear stress constant while reducing the effective
 184 stress (Reimer, 1992) (Fig. 6). Stress conditions for the
 185 laboratory testing were selected to approximate field
 186 conditions. The rate of strain was limited in the samples
 187 such that a large number of volumetric strain data were
 188 collected after the sample had reached the failure state.

189 3. Results

190 The mean topographic index of the debris flows and
 191 the slumps (Table 1) are not statistically different (t -test:
 192 $\alpha=0.05$), suggesting that differences in soil moisture
 193 from subsurface flow might not explain the different
 194 types of failure behavior. Nonetheless, the spatial het-
 195 erogeneity of the lithology could have caused pooling of
 196 water behind patches of soil that had relatively lower
 197 hydraulic conductivities.

The mean porosities of the two sets of failures (Table
 1) did not show a statistical difference (t -test: $\alpha=0.05$),
 suggesting that the two failure types cannot be distin-
 guished on the basis of porosity. This result, however, is
 not conclusive because soils with different particle size
 distributions may have different critical porosities (Fear
 and Robertson, 1995). Nevertheless, this strongly sug-
 gests that the initial porosity of a soil may not always be
 a reliable indicator of its liquefaction potential, a con-
 clusion also reached by Yamamuro and Lade (1998).

The results from the texture analysis indicate that the
 soils are sandy clay loams. The soils that mobilized as
 debris flows were significantly sandier than the slumps
 (t -test: $\alpha=0.05$) with a sand content of $\sim 45\%$ sand
 distinguishing the two types of failures (Fig. 7; Table
 1). This supports the common observation that differ-
 ences in the fines/sand ratio may result in fundamental
 differences in shearing behavior (Xenaki and Athana-
 sopolous, 2003).

In all CSD tests, the effective normal stress was
 reduced until failure. Initial and failure stress states
 are shown in Table 2. No attempt at defining a failure
 envelope was made because the samples, from different

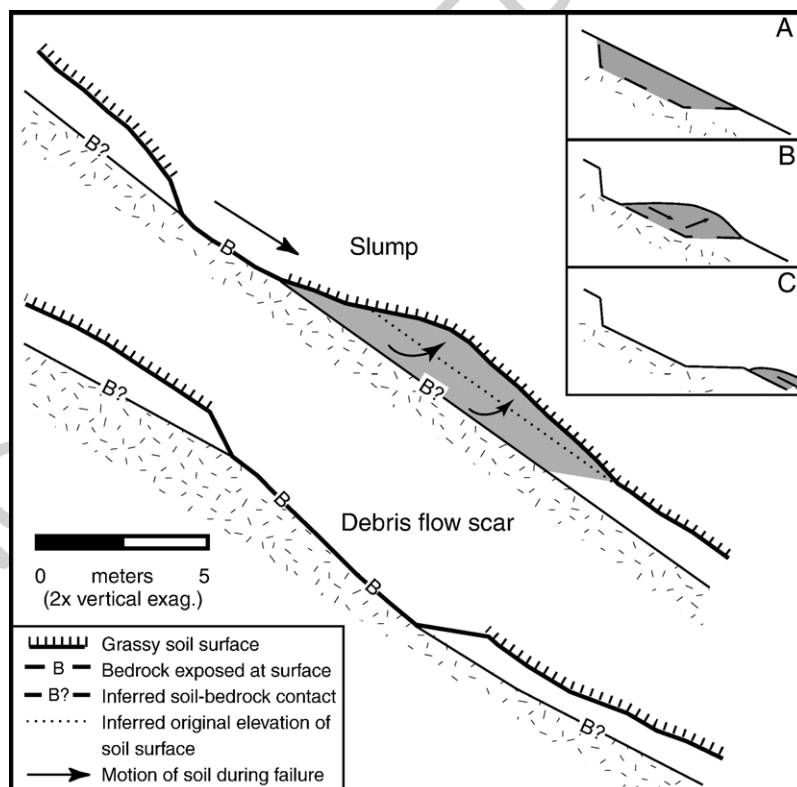


Fig. 5. Surveyed longitudinal profiles of a slump (SF100; top) and debris flow scar (DF9; bottom). Inset: Sequence leading to slumps and debris flows. (A) Incipient landslide (shaded) and failure planes (dashed line). (B) Failure begins at the upper scarp. In some failures, movement was arrested and these formed slumps. (C) Others mobilized as debris flows, completely evacuating the scar.

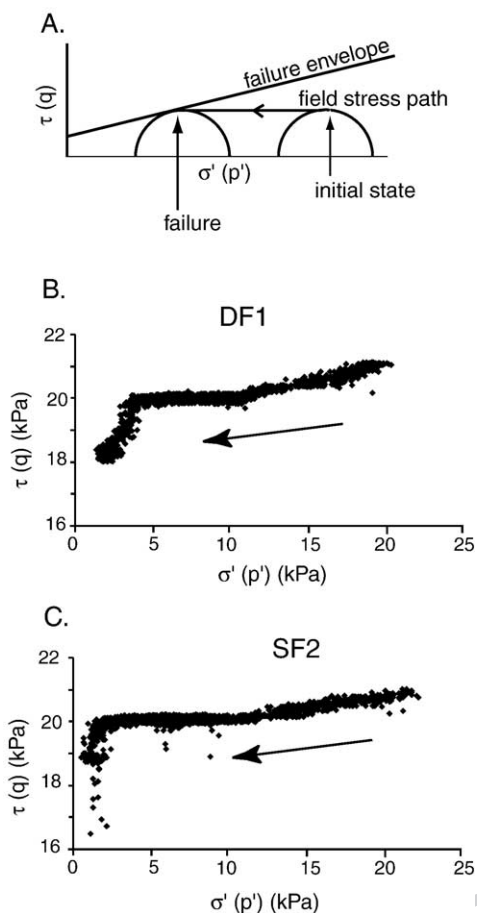


Fig. 6. (A) Stress path for the CSD tests. (B, C) Stress paths for two soil samples representing a soil that liquified (DF1) and one that did not (SF2). Arrows indicate the direction of the stress paths.

221 sites, were considered to be composed of different
 222 material with different material properties (e.g., varying
 223 particle size distributions, Fig. 7). Unexpectedly, the
 224 CSD tests revealed that the soils in both the slumps
 225 and the debris flows were dilational under ambient field
 226 conditions (Fig. 8). The volumetric increase of the soils

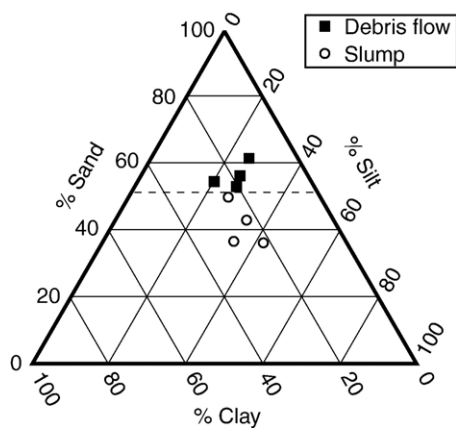


Fig. 7. Soil textures of the slumps and the debris flows. The soils with sand >45% produced debris flows, whereas the less sandy soils only slumped.

during shear is evidence that they were dilating as the 244
 soil particles rode up and over each other. But if the 245
 increase in pore pressure that leads to liquefaction can 246
 only be generated in a soil that contracts, then how does 247
 a dilative soil reach a contractive state? 248

4. Discussion 249

4.1. Liquefaction of dilative soils 250

Because CSD testing is complex, requires special- 251
 ized equipment, and is labor-intensive, only a few 252
 studies have applied the CSD test to colluvial soils. 253
 Anderson and Reimer (1995) tested a series of colluvial 254
 soil samples from the San Francisco Bay Area and 255
 observed that they all dilated. In an investigation of 256
 debris flow initiation, Anderson and Sitar (1995) per- 257
 formed CSD tests on undisturbed soil samples from 258
 hillslopes that had numerous debris flows and also 259
 found that the soils were dilative. Field experiments 260
 by Harp et al. (1990) have also shown soils dilating 261
 during failure. In fact, Anderson and Sitar (1995) con- 262

t.1.1 Table 1
 t.1.2 Comparison of the sites and soils between slumps and debris flows

t.1.3	Failure type	Sample	Slope (°)	Topographic index	Porosity	% Sand
t.1.4	Slumps	SF1	31	3.6	0.55	39
t.1.5		SF2	29	4.5	0.48	32
t.1.6		SF100	29	5.3	0.50	32
t.1.7		SF101	28	5.1	0.48	44
t.1.8		Ave. ± 1 S.D.	29.3 ± 1.3	4.6 ± 0.8	0.50 ± 0.04	37 ± 6
t.1.9	Debris flows	DF1	29	5.1	0.53	51
t.1.10		DF6	29	4.6	0.48	47
t.1.11		DF9	30	4.3	0.56	49
t.1.12		DF100	32	5.1	0.51	58
t.1.13		Ave. ± 1 S.D.	30.0 ± 1.4	4.8 ± 0.4	0.52 ± 0.03	51 ± 5

t2.1 Table 2
t2.2 Initial and final stresses for CSD tests

t2.3	Sample	Initial σ'	Initial τ	σ' at failure
t2.4	SF1	28.1 ± 0.2	30.4 ± 0.1	3.4 ± 0.1
t2.5	SF2	19.4 ± 0.6	21.0 ± 0.2	3.8 ± 0.3
t2.6	DF1	21.3 ± 0.4	20.8 ± 0.2	1.7 ± 0.3

t2.7 The testing apparatus experienced some variability in stress readings, values are averages over 5 min, errors are 1 S.D. Time and state of failure is approximate due to variability in stresses through the testing. Data file for SF6 was corrupted and we were unable to recover some data.

263 clude that most, if not all, natural colluvial soils will
264 dilate under the stress conditions found in shallow
265 landslides.

266 It is generally accepted that liquefaction only
267 occurs in soils that have a porosity greater than the
268 critical-state porosity (Casagrande, 1936) and that
269 liquefaction of hillslope soils during storm events
270 leads to debris flows (Iverson et al., 2000). In soils
271 well above the critical-state porosity, liquefaction will
272 occur immediately upon slope failure (Iverson et al.,
273 2000). Less well understood is the mechanism by
274 which a soil in an initially dense and dilative state
275 transforms into a contractive soil that may then
276 collapse catastrophically.

277 Several studies have proposed a mechanism to
278 explain the mobilization of debris flows from dilative
279 soils. Fleming et al. (1989) and Dai et al. (1999a,b)
280 hypothesized that the landslide slides forward a limited
281 distance and stops, its motion inhibited by the
282 dilation of the soil and the concomitant decrease in
283 pore pressure. The soil, now looser and in a dilative
284 state, absorbs water either from continued rainfall or
285 from water ponding behind the slump (Harp et al.,
286 1990, 2004). As the slumped mass resaturates, pore
287 pressures climb once again, initiating a second failure.
288 Because the soil is now in a dilative state, this second
289 failure leads to the contraction of the soil that pro-
290 duces the rapid spike in pore pressure necessary for
291 liquefaction. This process may include a pause that
292 has been noted in eyewitness accounts. For example,
293 Ellen et al. (1989) provided descriptions of failures
294 that mobilized as debris flows only after a period of
295 time had elapsed after the initial failure. In an analysis
296 of landslides triggered by a typhoon, Harp et al.
297 (2004) reported several instances where the landslide
298 initially failed as a slump, impounded water draining
299 from upslope, and then catastrophically failed as a
300 debris flow. A field experiment by Harp et al.
301 (1990) also produced this type of behavior. Below,

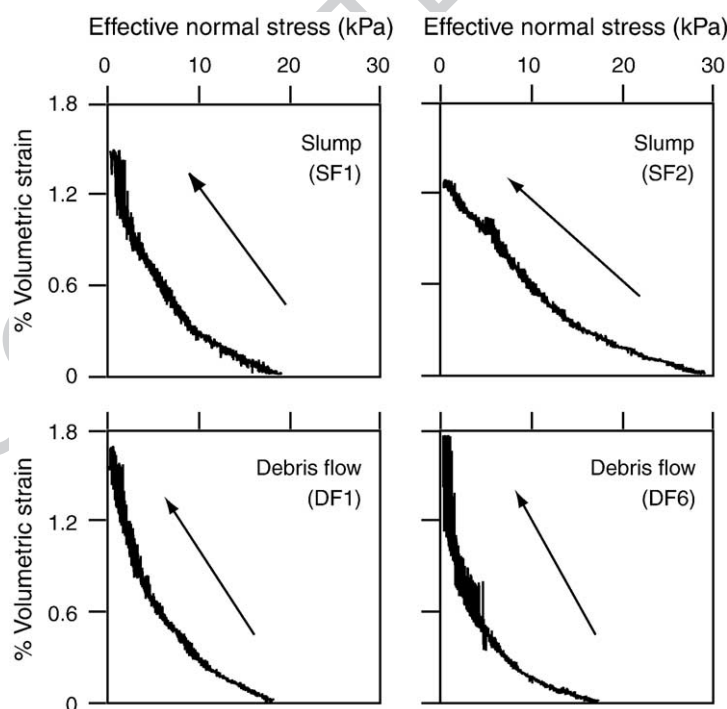


Fig. 8. Results from the CSD tests. Arrows indicate the stress paths. The soil samples representing the slumps, SF1 and SF2, exhibited an increase in volumetric strain with a reduction in effective stress, indicating that the soils dilated during shear. Surprisingly, samples from the debris flow sites, DF1 and DF6, were also dilative.

302 we investigate this mechanism with a numerical
303 model.

304 4.2. Numerical model

305 Iverson (2005) presented a model which couples the
306 motion of a sliding block with a parsimonious descrip-
307 tion of pore water pressures within the block that
308 respond to dilation or collapse of the soil matrix. We
309 combine this model with critical state theory to inves-
310 tigate the mobilization process described above. The
311 motion of the fault block can be described by a balance of
312 driving and resisting forces (Iverson, 2005):

$$\frac{1}{g} \frac{d^2}{u_x dx^2} = \cos^2 \Psi [\sin(\theta - \Psi) - \left(\cos(\theta - \Psi) - \frac{p(0, t)}{\rho g H} \cos \Psi \right) \tan \phi] \quad (3)$$

314 where g ($L T^{-2}$) is gravitational acceleration, u_x (L) is
315 the downslope displacement of the failure block, Ψ is
316 the dilation angle, θ is the slope angle, ϕ is the friction
317 angle, p ($M T^{-2} L^{-1}$) is the pore pressure at the base of
318 the slide block, ρ ($M L^{-3}$) is the density of the slide
319 block, and H is the thickness of the slide block. The
320 dilation angle, Ψ , is defined as $\Psi = du_y / du_x$ where u_y
321 (L) is the vertical displacement due to dilation or con-
322 traction of the shear zone.

323 Following Iverson (2005), the pore pressure at the
324 base of the slide block, $p(0, t)$, is the sum of an imposed
325 pressure, p_i , which is due to rain infiltration, and an
326 excess pore pressure, p_e , which is due to the dilation or
327 contraction of the soil, such that $p = p_i + p_e$. Both the
328 excess and imposed pore pressures obey the diffusion
329 equation: $\partial p_{i,e} / \partial t = D \partial^2 p_{i,e} / \partial z^2$, where D ($L^2 T^{-1}$) is
330 the hydraulic diffusivity. The excess pore pressure
331 obeys two boundary conditions: 1) it is zero at the
332 top of the water table (a distance z above the top of
333 the shear zone, measured normal to the failure plane)
334 and, 2)

$$\frac{\partial p_e}{\partial z}(0, t) = \frac{\rho_w g}{K} \psi v \quad (4)$$

336 where ρ_w ($M L^{-3}$) is the density of water, K ($L T^{-1}$) is
337 the saturated hydraulic conductivity, and $v = du_x / dt$ is
338 the velocity of the slide block (Iverson, 2005). The
339 location $z=0$ corresponds to the top of the shearing
340 surface. The imposed pore pressure is increased linearly
341 in the simulations following Iverson (2005) according to
342 $p_i(t) = p_{crit} + WKZD^{-1}t$, where p_{crit} is the critical pressure
343 required for downslope motion to commence (e.g., the
344 pressure when $d^2u/dx^2=0$) and W is a dimensionless
345 rate of imposed pore pressure increase. Eq. (3) is solved
346 using the numerical method described by Iverson
347 (2005), and the equation governing the diffusion of
348 excess pore pressure is solved with a fully implicit
349 finite difference method (Smith, 1986). Our model

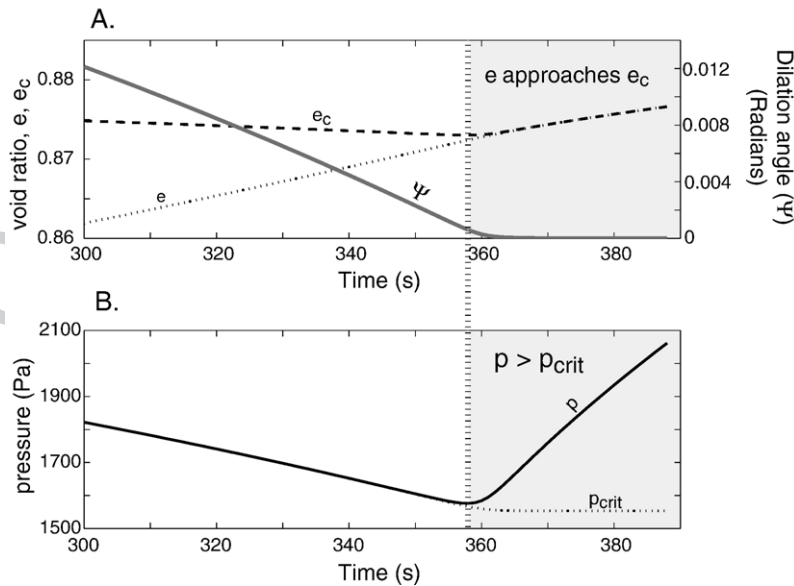


Fig. 9. (A) Period shortly before and after critical void ratio (e_c) is reached in the shear zone of a sliding block. Model parameters listed in Table 3. As e approaches e_c , the dilation angle Ψ approaches zero. (B) As Ψ approaches zero, the basal pore pressure p grows beyond the critical pore pressure p_{crit} necessary to cause downslope motion.

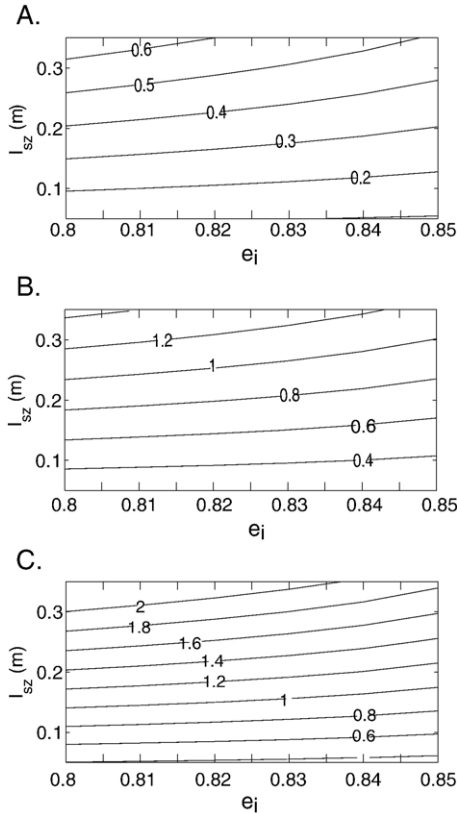


Fig. 10. Downslope displacement (in meters) required for void ratio e to come to within a threshold value of 0.0001 of the critical void ratio e_c as a function of the shear zone thickness, the initial void ratio (critical void ratio in these simulations was ~ 0.87), and γ . (A) $\gamma=0.05$. (B) $\gamma=0.1$. (C) $\gamma=0.15$. Parameter values for these simulations given in Table 3.

differs from that of Iverson (2005) in our treatment of the dilation angle, Ψ , as described below. In addition, we track the evolution of the void ratio in order to extend the analysis to include critical state theory.

It has been found that Ψ changes as the shear zone void ratio approaches the critical state (Li, 1997). As the void ratio in the shear zone approaches the critical void ratio, Ψ will approach zero. In our simulations, Ψ is determined by

$$\psi = \text{sgn}(e_c - e)\psi_0 \left(1 - e^{\frac{e_c - e}{\gamma}}\right) \quad (5)$$

where $\text{sgn}(e_c - e)$ returns the value 1 if $e_c - e > 0$ and -1 if $e_c - e < 0$, Ψ_0 is the initial dilation angle, e is the void ratio, e_c is the critical void ratio, and γ is a dimensionless material constant that determines how quickly Ψ approaches zero as the shear zone approaches the critical void ratio. The critical void ratio, e_c , is a function of the effective mean stress (Verdugo and Ishihara, 1996), which can be modeled as

$$e_c = e_0 - \lambda \left[\frac{\rho g H \cos \theta - p(0, t)}{p_A} \right]^\zeta \quad (6)$$

where p_A ($\text{M T}^{-2} \text{L}^{-1}$) is atmospheric pressure and e_0 , λ , and ζ are dimensionless material constants. The change in void ratio of the shear zone will depend on its thickness, l_{sz} (L). We assume that there is no volumetric expansion or contraction of the shear zone in the slope parallel direction, such that the volumetric strain is accommodated only by vertical expansion or con-

Table 3
Values used to generate Figs. 10 and 11

Parameter	Values used to generate Fig. 10	Values used to generate Figs. 10 and 11A	Values used to generate Fig. 11B
θ	31°	31°	31°
ϕ	35°	35°	35°
Ψ_0	6°	6°	6°
ρ	2000 kg m^{-3}	2000 kg m^{-3}	2000 kg m^{-3}
ρ_w	1000 kg m^{-3}	1000 kg m^{-3}	1000 kg m^{-3}
D	$3 \times 10^{-3} \text{ m}^2 \text{ s}^{-1}$	$3 \times 10^{-3} \text{ m}^2 \text{ s}^{-1}$	$5 \times 10^{-3} \text{ m}^2 \text{ s}^{-1}$
K	$2 \times 10^{-5} \text{ m s}^{-1}$	$2 \times 10^{-5} \text{ m s}^{-1}$	$2 \times 10^{-6} \text{ m s}^{-1}$
H	0.65 m	0.65 m	0.65 m
Z	0.46 m	0.46 m	0.46 m
\ddot{e}	0.47	0.47	0.47
e_0	1.01	1.01	1.01
ζ	0.5	0.5	0.5
e_i	Varies	0.82	0.82
γ	Varies	0.1	0.1
l_{sz}	Varies	0.1 m	0.1 m

Parameters for Eqs. (1) and (2) selected to be similar to those used by Iverson (2005 #499) Parameters used for Eq. (4) chosen to approximate the soil studied by Anderson and Reimer (1995 #288). We do not use our measurements to constrain the simulations as we consider each sample to be a different material (due to differences in particle size distribution).

377 traction. In such a case the void ratio, e , is related to the
378 initial void ratio e_i , by

$$e = e_i + \frac{u_y}{l_{sz}}(1 + e_i). \quad (7)$$

380 **Iverson (2005)** found that if the dilation angle Ψ is
382 allowed to decay with increasing downslope motion, a
383 sliding block whose shear zone begins in a dilative state
384 may exhibit behavior similar to the liquefaction behav-
385 ior that accompanies a sliding block whose shear zone
386 begins in a contractive state. Our model reproduces
387 these results, but we explicitly model the decay of the
388 dilation angle based on the relation of the void ratio in
389 the shearing layer to the critical void ratio. As the shear
390 zone dilates during failure, negative pore pressures are
391 maintained which arrest the downslope movement of
392 the sliding block. When the void ratio in the shear zone
393 approaches the critical void ratio, however, the reduced
394 dilation can no longer dissipate the pressure being
395 generated in the shear zone (Fig. 9), leading to the
396 rapid acceleration of the slide block.

397 Using the numerical model, we examined the down-
398 slope displacement necessary for the void ratio to ap-
399 proach to within a threshold of the critical void ratio
400 ($e_c - e > 0.0001$), and found that relatively little dis-
401 placement ($\sim 10^{-1}$ – 1.0^0 m) is needed for the shear
402 zone to approach the critical state porosity (Fig. 10).
403 The values of Ψ/Ψ_0 at the threshold void ratio
404 ($e_c - e > 0.0001$) ranged from 1.4×10^{-3} to

3.5 $\times 10^{-3}$, therefore the equivalent u_{xref} distances
used by **Iverson (2005)** are much smaller than the
displacement distances to the threshold void ratio. We
chose the threshold void ratio because this was the
approximate difference between the void ratio and crit-
ical void ratio at which rapid acceleration began in our
simulations. The parameter values for these simulations
are shown in Table 3.

If relatively little downslope displacement is needed
to achieve the critical void ratio for even very densely
packed soils, why did some of the failures at Sedgwick
Ranch mobilize and others did not? We suggest that the
difference in behavior is due to the particle size distri-
bution of the soils (Fig. 7). The rate at which the shear
zone of a failing block can dilate depends fundamen-
tally on the rate at which water can be forced into the
dilating area through negative pore pressures generated
in the shear zone. This rate of dilation will determine
how quickly a failing soil can approach the critical state
porosity. Because sandier soils have greater hydraulic
conductivities (Fetter, 1997), pore water in these soils
will be able to flow into the dilating shear zone at a
faster rate than in clay rich soils, thus a sandy slide
block will be able to dilate and approach the critical
void ratio more rapidly. In the case of the clay rich
slumps, the elevated pore pressures necessary to cause
failures induced by rainstorms presumably did not last
for a great enough period of time for the slump block to
reach the critical void ratio. To illustrate the effect of

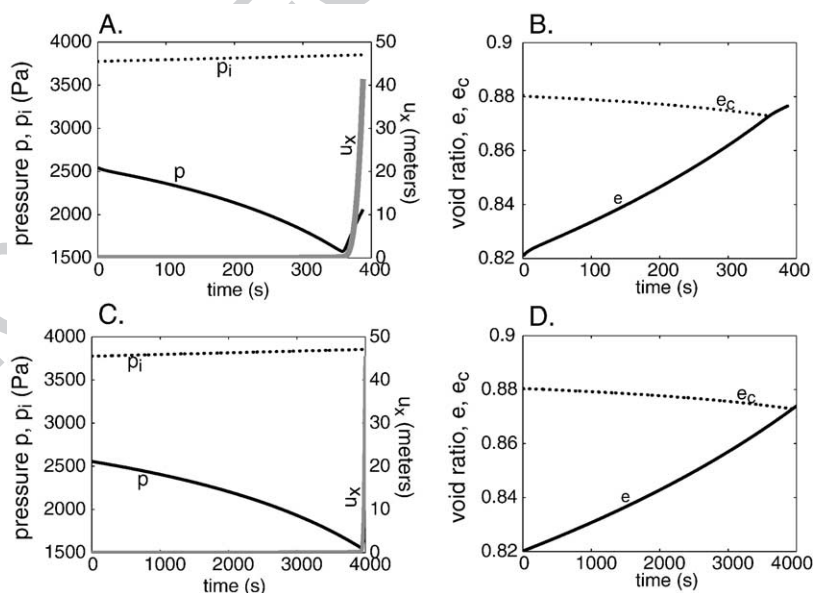


Fig. 11. Simulations of two soils with different saturated hydraulic conductivities. (A, B) $K = 2 \times 10^{-5} \text{ m s}^{-1}$. (C, D) $K = 2 \times 10^{-6} \text{ m s}^{-1}$. An order of magnitude reduction in K leads to an order of magnitude increase in the time elapsed between commencement of failure and rapid downslope acceleration. Note different scales on x-axes. Parameter values listed in Table 3.

434 hydraulic conductivity on the rate of change in the void
 435 ratio, we simulated two failing blocks with different
 436 hydraulic conductivities. The simulations indicate that a
 437 tenfold decrease in hydraulic conductivity results in an
 438 equivalent increase in the time elapsed between the
 439 initiation of failure and rapid downslope acceleration
 440 (Fig. 11). The observation that sandier soils are more
 441 apt to liquefy has often been made by others; and it is
 442 generally agreed (with some exceptions) that liquefac-
 443 tion potential increases with sand content (Xenaki and
 444 Athanasopoulos, 2003).

445 5. Conclusion

446 In this study, we examine the processes that trans-
 447 form rigid translational landslides into debris flows.
 448 Soils adjacent to shallow landslides were subjected to
 449 triaxial shear tests designed to simulate realistic
 450 changes in the stress field during failure. The results
 451 indicate that debris flows mobilized in soils that were
 452 dilative under ambient field conditions, an unexpected
 453 finding given current theory on debris flow mobiliza-
 454 tion. With a numerical model, we explore the condi-
 455 tions under which a dilative soil may approach the
 456 critical void ratio. We conclude that a particular site's
 457 potential for debris flow mobilization was independent
 458 of porosity but sensitive to sand content.

459 Acknowledgements

460 We are indebted to M. Reimer for his help with the
 461 CSD tests and for access to the U.C. Berkeley Geo-
 462 technical Laboratory. Thanks are also due to O. Chad-
 463 wick and W. Lick for access to their facilities. T.
 464 Dunne is thanked for discussions. D. Petley, E.
 465 Harp, S. Lancaster, R. Moss, R. Iverson, M. Reid,
 466 and anonymous reviewer are thanked for comments on
 467 earlier drafts. Supplies and salary for EG were sup-
 468 ported by U.C. Water Resources Grant UCAL-W-917,
 469 a Sigma Xi grant, and a Mildred Mathias grant. SM
 470 was supported by a George Tunnel Memorial Fellow-
 471 ship granted by the UCSB department of Geological
 472 Sciences.

473 References

474

475 Alexander, D., 1989. Urban landslides. *Progress in Physical Geogra-*
 476 *phy* 13, 157–191.
 477 Anderson, S.A., Reimer, M.F., 1995. Collapse of saturated soil due to
 478 reduction in confinement. *Journal of Geotechnical Engineering*
 479 121 (2), 216–220.
 480 Anderson, S.A., Sitar, N., 1995. Analysis of rainfall-induced debris
 481 flows. *Journal of Geotechnical Engineering* 121 (7), 544–552.

Benda, L., Dunne, T., 1997. Stochastic forcing of sediment routing 482
 and storage in channel networks. *Water Resources Research* 33, 483
 2849–2863. 484
 Benda, L., Miller, D., Bigelow, P., Andras, K., 2003. Effects of post- 485
 wildfire erosion on channel environments, Boise River, Idaho. 486
Forest Ecology and Management 178, 105–119. 487
 Beven, K., Kirkby, M.J., 1979. A physically-based variable contrib- 488
 uting area model of catchment hydrology. *Hydrological Sciences* 489
Bulletin 24 (1), 43–69. 490
 Brasher, B.R., Franzmeier, D.P., Valassis, V., Davidson, S.E., 1966. 491
 Use of Saran resin to coat natural solid clods for bulk-density and 492
 water retention measurements. *Soil Science* 101, 108. 493
 Casagrande, A., 1936. Characteristics of cohesionless soils affecting 494
 the stability of slopes and earth fills. *Journal of the Boston Society* 495
of Civil Engineers 23 (1), 13–32. 496
 Dai, F., Lee, C.F., Sijing, W., 1999a. Analysis of rainstorm-induced 497
 slide-debris flows on natural terrain of Lantau Island, Hong Kong. 498
Engineering Geology 51, 279–290. 499
 Dai, F., Lee, C.F., Wang, S., Feng, Y., 1999b. Stress–strain behav- 500
 iour of a loosely compacted volcanic-derived soil and its sig- 501
 nificance to rainfall-induced fill slope failures. *Engineering* 502
Geology 53, 359–370. 503
 Dibblee, T.W.J., 1993. Geologic map of the Los Olivos Quadran- 504
 gle, #DF-44. Dibblee Geological Foundation, Santa Barbara, 505
 California. 506
 Doraiswamy, D., et al., 1991. The Cox–Merz rule extended: a rheo- 507
 logical model for concentrated suspensions and other materials 508
 with a yield stress. *Journal of Rheology* 35 (4), 647–685. 509
 Ellen, S.D., Cannon, S.H., Reneau, S.L., 1989. Distribution of 510
 debris flows in Marin County. USGS Professional Paper 511
 1434, 113–131. 512
 Fear, C.E., Robertson, P.K., 1995. Estimating the undrained strength 513
 of sand: a theoretical framework. *Canadian Geotechnical Journal* 514
 32, 859–870. 515
 Fetter, C.W., 1997. *Applied Hydrogeology*. Macmillan College Pub- 516
 lishing Company, New York. 691 pp. 517
 Fleming, R.W., Ellen, S.D., Aligus, M.A., 1989. Transformation of 518
 dilative and contractive landslide debris into debris flows—an 519
 example from Marin County, California. *Engineering Geology* 520
 27, 201–223. 521
 Gabet, E.J., Dunne, T., 2002. Landslides on coastal sage-scrub and 522
 grassland hillslopes in a severe El Nino winter: the effects of 523
 vegetation conversion on sediment delivery. *Geological Society of* 524
America Bulletin 114 (8), 983–990. 525
 Gabet, E.J., Dunne, T., 2003. A stochastic sediment supply model for 526
 a steep Mediterranean landscape. *Water Resources Research* 39 527
 (9), 1237; doi: 10.1029/2003WRR002341. 528
 Gares, P.A., Sherman, D.J., Nordstrom, K.F., 1994. Geomorphology 529
 and natural hazards. *Geomorphology* 10, 1–18. 530
 Harp, E.L., Wells, W.G., Sarmiento, J.G., 1990. Pore pressure re- 531
 sponse during failure in soils. *Geological Society of America* 532
Bulletin 102 (4), 428–438. 533
 Harp, E.L., Reid, M.R., Michael, J.A., 2004. Hazard Analysis of 534
 Landslides Triggered by Typhoon Chata'an on July 2, 2002, in 535
 Chuuk State, Federated States of Micronesia, USGS Open-File 536
 Report 2004-1348US Dept. of the Interior, Washington, DC. 537
 Iverson, R.M., 2005. Regulation of landslide motion by dilatancy and 538
 pore pressure feedback. *Journal of Geophysical Research-Earth* 539
Surface 110 (F2); doi: 10.1029/2004JF000268. 540
 Iverson, R.M., Reid, M.E., LaHusen, R.G., 1997. Debris-flow mobi- 541
 lization from landslides. *Annual Review of Earth and Planetary* 542
Sciences 25, 85–138. 543

- 544 Iverson, R.M., et al., 2000. Acute sensitivity of landslide rates to
545 initial soil porosity. *Science* 290, 513–516.
- 546 Johnson, A.D., 1996. A Model for Grain Flow and Debris Flow.
547 USGS Open-File Report, vol. 96-728. US Dept. of the Interior,
548 Denver, CO.
- 549 Kesseli, J.E., 1943. Disintegrating soil slips of the coast
550 ranges of central California. *The Journal of Geology* 11 (5),
551 342–352.
- 552 Li, X.S., 1997. Modeling of dilative shear failure. *Journal of Geo-*
553 *technical and Geoenvironmental Engineering* 123 (7), 609–616.
- 554 Reimer, M.F., 1992. The effects of testing conditions on the consti-
555 tutive behavior of loose, saturated sands under monotonic loading.
556 PhD thesis, University of California, Berkeley.
- 557 Sassa, K., 1984. The mechanism starting liquified landslides and
558 debris flows. 4th International Symposium on Landslides. Inter-
559 national Society for Soil Mechanics and Foundation Engineering,
560 Toronto, Ontario, pp. 349–354.
- 576
- Smith, G.D., 1986. *Numerical Solution of Partial Differential Equa-*
561 *tions: Finite Difference Methods.* Oxford University Press, Ox-
562 ford. 350 pp.
- Stock, J., Dietrich, W.E., 2003. Valley incision by debris flows:
563 evidence of a topographic signature. *Water Resources Research*
564 39 (4), 1089; doi: 10.1029/2001WR001057. 566
- Verdugo, R., Ishihara, K., 1996. The steady state of sandy soils. *Soil*
567 *and Foundation* 36 (2), 81–91. 568
- Xenaki, V.C., Athanasopolous, G.A., 2003. Liquefaction resistance
569 of sand-silt mixtures: an experimental investigation of the
570 effect of fines. *Soil Dynamics and Earthquake Engineering* 23,
571 183–194. 572
- Yamamuro, J.A., Lade, P.V., 1998. Steady-state concepts and static
573 liquefaction of silty sands. *Journal of Geotechnical and Geoenvir-*
574 *onmental Engineering* 124 (9), 868–877. 575

UNCORRECTED PROOF